

INFLUENCE OF HEAD SHAPE ON MEASURED ACTIVITY OF ACTINIDES

T.Vrba¹

¹ Czech Technical University in Prague, Faculty of Nuclear Sciences and Physical Engineering,
Brehova 7, 11519 Prague, Czech Republic

Abstract: In vivo measurement of actinides activity in human skull is a valuable technique of internal dosimetry. Many articles were published on calibrations and some new facts were found. The most important finding was that the relation of measured head size and size of a calibration phantom has notable effect on measured activity; however real impact depends on the detectors geometry. Still opened and never studied issue is: How variation in the head shape influences measured activity. Current study tries to provide answer to this question by the means of Monte Carlo simulation and voxel phantoms.

Keywords: voxel phantom, in vivo, ²⁴¹Am, skull, calibration

1 Introduction

Detection systems for in-vivo measurement of radionuclides incorporated in a human body have to be calibrated in order to provide quantitative results. One of the widely used methods for measurement of the bone seeking radionuclides is skull gamma spectrometry measurement with germanium detectors. Important question of the technique is its uncertainty. There were performed some analyses on possible source of the uncertainty, such as activity distribution, detector placement, and skull size (1) (2) (3). Such studies are usually performed with a voxel phantom and particle transport is handled by Monte Carlo method. Effect of head size was studied only via voxel side scaling in isotropic way for one measurement configuration and rather small detectors. Current paper tries to outline possible effect of a head shape on detection efficiency for eight detector positions. The paper also compares newly available phantoms developed by ICRP for dosimeter calculation with previously developed head phantom (2).

2 Materials and method

2.1 Phantoms

Three different anthropomorphic models of human head were used in the paper. The first two were heads of ICRP reference voxel phantoms of male and female. These phantoms were constructed in order to replace analytical models, of the man in dose calculations. Detailed information on the phantoms is in ICRP Recommendation 110 (4). Third phantom was built in 2007 from CT images of a 38 year old woman (2). Three bone tissues with different densities and four soft tissues were segmented from the original data. Bone regions were attributed to three parts of the skeleton, i.e. cranium, mandible with teeth and neck vertebra. Moreover bone voxels on surface were identified separately in

order to allow imitation of the distribution used in artificially labeled phantoms with ^{241}Am . The phantom will be denoted as Linda in the rest of the paper. Simplified model of Linda phantom were made in order to facilitate simulation. Simplified model decrease resolution by two and replace various bone and soft tissues with their mean. Such change reduced number of voxel to the reasonable level and avoid blurring from scaling. Size of the phantoms was compared via head mean radius R. Mean head radius is half of arithmetic average of head diameters as it shows in Figure 1.

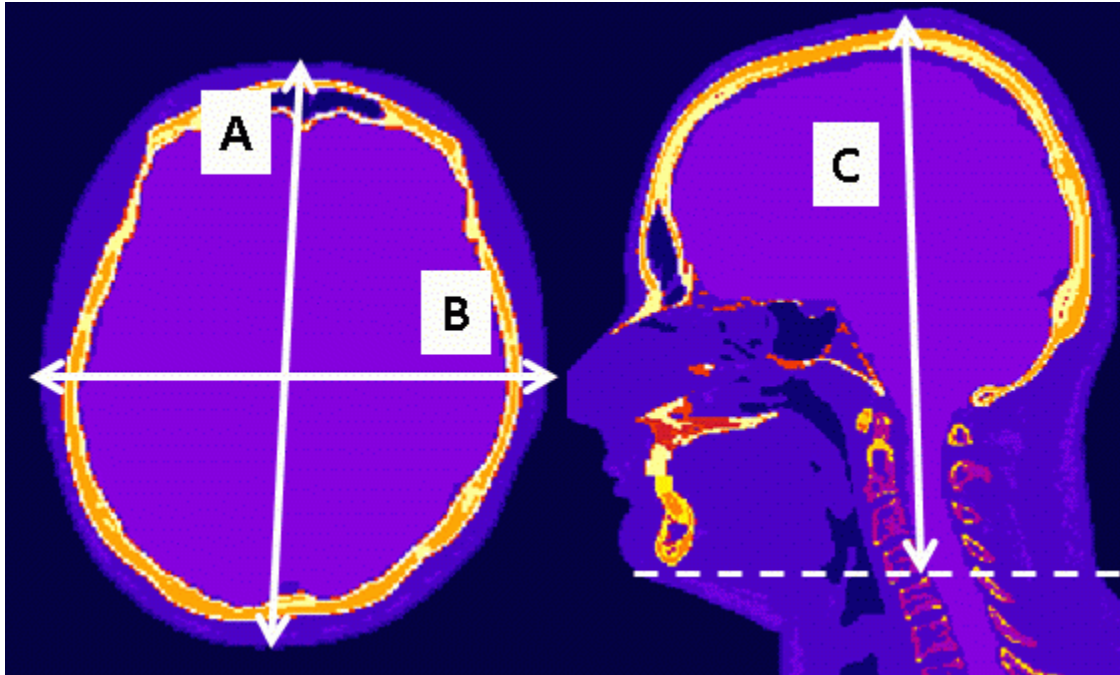


Figure 1 Dimension of the phantoms used for head mean radius calculation.

Mathematical expression is expressed in equation 1

$$R = \frac{A+B+C}{6} \quad \text{Equation 1}$$

where A, B, C are dimensions from the Figure 1. Comparison of the basic phantom properties is in .

Table 1 Basic information on the phantoms

| Phantom | Voxel side (mm) | | | Diameters(cm) | | | R (cm) | number of voxels |
|--------------|-----------------|------|------|---------------|-------|-------|--------|------------------|
| | x | y | z | A | B | C | | |
| ICRP female | 1.78 | 1.78 | 4.84 | 20.47 | 14.86 | 21.30 | 9.44 | 715950 |
| ICRP male | 2.14 | 2.14 | 8.00 | 21.08 | 16.44 | 22.40 | 9.98 | 399156 |
| Linda | 1.00 | 1.00 | 1.00 | 18.70 | 16.00 | 21.70 | 9.40 | 11175868 |
| Linda simple | 2.00 | 2.00 | 2.00 | 18.70 | 16.00 | 21.70 | 9.40 | 1241550 |

2.2 Detector

Low energy germanium (LEGe) detectors of different size are often used for measurement of low energy emitters such as ^{241}Am . Model of detector (LX-70450-30-CW) manufactured by Ortec has been used in simulation. It has similar size and properties as Canberra GL3825R and thus is good representative. The detector model was based on the information from the manufacturer and unknown parts of the model were adjusted by real measurement data. Basic characteristics of the detector and comparison with GL3825R are in

Table 2.

Table 2 Detector comparison

| property | Canberra (GL3825R) | Ortec [*] (LX-70450-30CW) ^a | Current model |
|---------------------------------|-----------------------|--|------------------|
| diameter (mm) | 70 | 70 | 69.8 |
| depth (mm) | 25 | 30 | 30.5 |
| thickness of the window (mm) | 0.6 | 0.6 | 0.6 |
| FWHM @ 5.9 keV (eV) | 475 | 450 | n/a |
| FWHM @ 122 keV (eV) | 750 | 725 | 730 |
| crystal to window distance (mm) | 5 | 4 | 4 |

* General data sheet

2.3 Geometry

The model of the detector was arranged in eight positions around phantoms. The positions were chosen with the respect to real measurement geometries (5) except for positions no. 2. Distance of the detector to the head was assessed on the axis which intersects center of the detector window and aims against the head. Information on detector positions are summed in Table 3 and depicted in Figure 2. The difficulties with the reproducibility and accuracy will be discussed lately.

Table 3 Description of detector position

| Position no. | distance to head (cm) | description* |
|--------------|-----------------------|--|
| 1 | 1 | above skull circa 1-2 cm posteriorly from Bergma |
| 2 | 1 | pointing bottom part of occipital bone |
| 3 | 3 | left temporal bone |
| 4 | 3 | right temporal bone |
| 5 | 1 | between frontal and left parietal bone , angle 52° |
| 6 | 1 | between frontal and right parietal bone, angle -52° |
| 7 | 1 | median part of the frontal bone |

| | | |
|---|---|---|
| 8 | 1 | between parietal bones above occipital bone |
|---|---|---|

* approximate

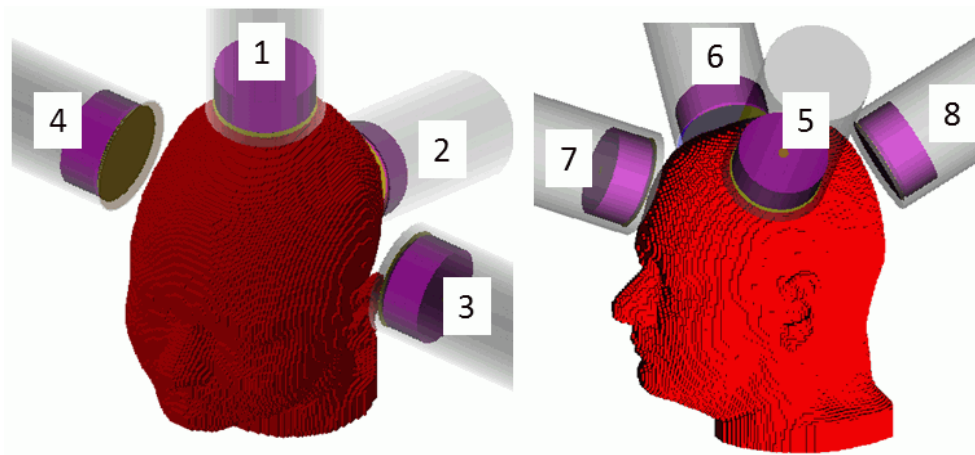


Figure 2 Detector positions

2.4 Size modification of simplified Linda phantom

Dimensions of the phantom were altered independently in all three directions. Sizing, expressed in the fraction of the original size, covers seven steps: (0.8, 0.9, 0.95, 1, 1.05, 1.1, 1.2), i.e. results in 343 configurations. Original phantom stored in analyze75 format was spitted in three subsets: skeletal, soft tissue and air region. Each subset were transferred to MATLAB and resized independently as binary objects, i.e. without interpolation. The resize procedure starts with planes (X and Y axis) and subsequently resizes volumes in perpendicular orientation (Y and Z axis). Bone subset was sampled in a way that tries to keeps same distance between outer surface of the phantom (skin) to bone, i.e. the thickness of the outlying tissue. All three subsets were merged back to the one volume. Merging process treat bone regions with the highest priority, followed by air structure (in the phantom) and the lowest importance was assign to soft tissue in a situation when voxel could be filled by more than one material. Position of the detector were adjusted to accord with new dimensioned the phantom. Thus distances were persevered, while coordinates and angles were modified. All resizing and adjusting operations were performed by a program written in MATAB.

3 Simulation

The simulations were performed in MCNPX version 2.6 (6). Primary particles used in simulations were monoenergetic photons with energy of 59.6 keV (^{241}Am), because detection efficiencies for this line are generally used for activity assessment. Other particles from ^{241}Am decay were omitted because they are not useful for calibration purposes, due to low emission and/or high attenuation. Number of primary particles (NPS) were 2×10^7 for the comparison of ICRP and Linda phantom which results in relative standard deviation (RSD) less that 0.4 % (highest value). Four times less NPS, i.e. 5×10^6 , were used for simulation with simplified Linda model in order to evaluate shape dependence of detection efficiency. Typical RSD were 0.5% while maximum was less than 0.75%. Default transport parameters for photons, i.e. detailed model, and standard electron straggling algorithm were used.

Gaussian energy broadening was not used in order to keep evaluation transparent. Tally F8 with bins size 0.5 keV covers region from 55 to 65 keV. Energy cut-off for non-detector cells (ELPT) was used in order to speed up simulation. Cut-off level for photon and electron was set to 57 keV thus it has no effect on simulated efficiency. Volume of all bone voxels belonging to cranium and mandible (with teeth) was treated as homogenous source.

4 Results

The efficiencies obtained from simulations, with modified simple Linda phantom, were plotted against mean had radius R. Figure 3 express dependency of the detection efficiency (in counts per Bq per second) a shows spread of the results due to different size proportions. Data for each detector position was fitted with power function and standard deviation of the data points was calculated. Results were aggregated in tTable 4.

Table 4 Results of the head shape variations

| Parameter | Detector position | | | | | | | |
|---|-------------------|---------|---------|---------|---------|---------|---------|---------|
| | 1 | 2 | 3 | 4 | 5 | 6 | 7 | 8 |
| Minimal e efficiency ^a | 2.0E-03 | 1.3E-03 | 1.5E-03 | 1.5E-03 | 2.4E-03 | 2.3E-03 | 2.3E-03 | 2.1E-03 |
| Maximal efficiency ^a | 4.6E-03 | 3.2E-03 | 3.1E-03 | 3.0E-03 | 5.1E-03 | 4.7E-03 | 4.6E-03 | 4.6E-03 |
| Fitting parameter A [*] | 0.2453 | 0.307 | 0.1335 | 0.1181 | 0.2407 | 0.1978 | 0.1711 | 0.2331 |
| Fitting parameter L [*] | 1.968 | 2.247 | 1.859 | 1.814 | 1.896 | 1.844 | 1.778 | 1.932 |
| Relative standard deviation due to head shape (%) | 10.5 | 7.0 | 10.1 | 10.2 | 6.0 | 7.0 | 3.5 | 3.5 |

* Parameter of the power functions from Figure 3

^aefficiency in counts×Bq⁻¹×s⁻¹

The comparison of the ICRP male and female phantom with Linda is depicted in Figure 4 and Table 5. Error bars in Figure 4 represents 10% interval, which is assumed, to be probable uncertainty of the detector placement. The assumption stands on previous study (3). Statistical error was not taken in account because its impact is marginal.

Table 5 Comparison of the detection efficiencies for studied phantom

| Detector position no. | Efficiency (counts×Bq ⁻¹ ×s ⁻¹) | | | |
|-----------------------|--|---------------------|-------------|-----------|
| | Linda | Linda -simple model | ICRP FEMALE | ICRP MALE |
| 1 | 3.02E-03 | 2.98E-03 | 3.98E-03 | 3.62E-03 |
| 2 | 1.98E-03 | 1.97E-03 | 2.17E-03 | 1.11E-03 |
| 3 | 2.09E-03 | 2.06E-03 | 2.05E-03 | 1.64E-03 |
| 4 | 2.01E-03 | 2.03E-03 | 2.08E-03 | 1.76E-03 |
| 5 | 3.46E-03 | 3.39E-03 | 3.15E-03 | 2.80E-03 |
| 6 | 3.11E-03 | 3.13E-03 | 3.21E-03 | 2.93E-03 |

| | | | | |
|---|----------|----------|----------|----------|
| 7 | 3.19E-03 | 3.13E-03 | 2.95E-03 | 2.82E-03 |
| 8 | 3.02E-03 | 3.03E-03 | 2.59E-03 | 2.58E-03 |

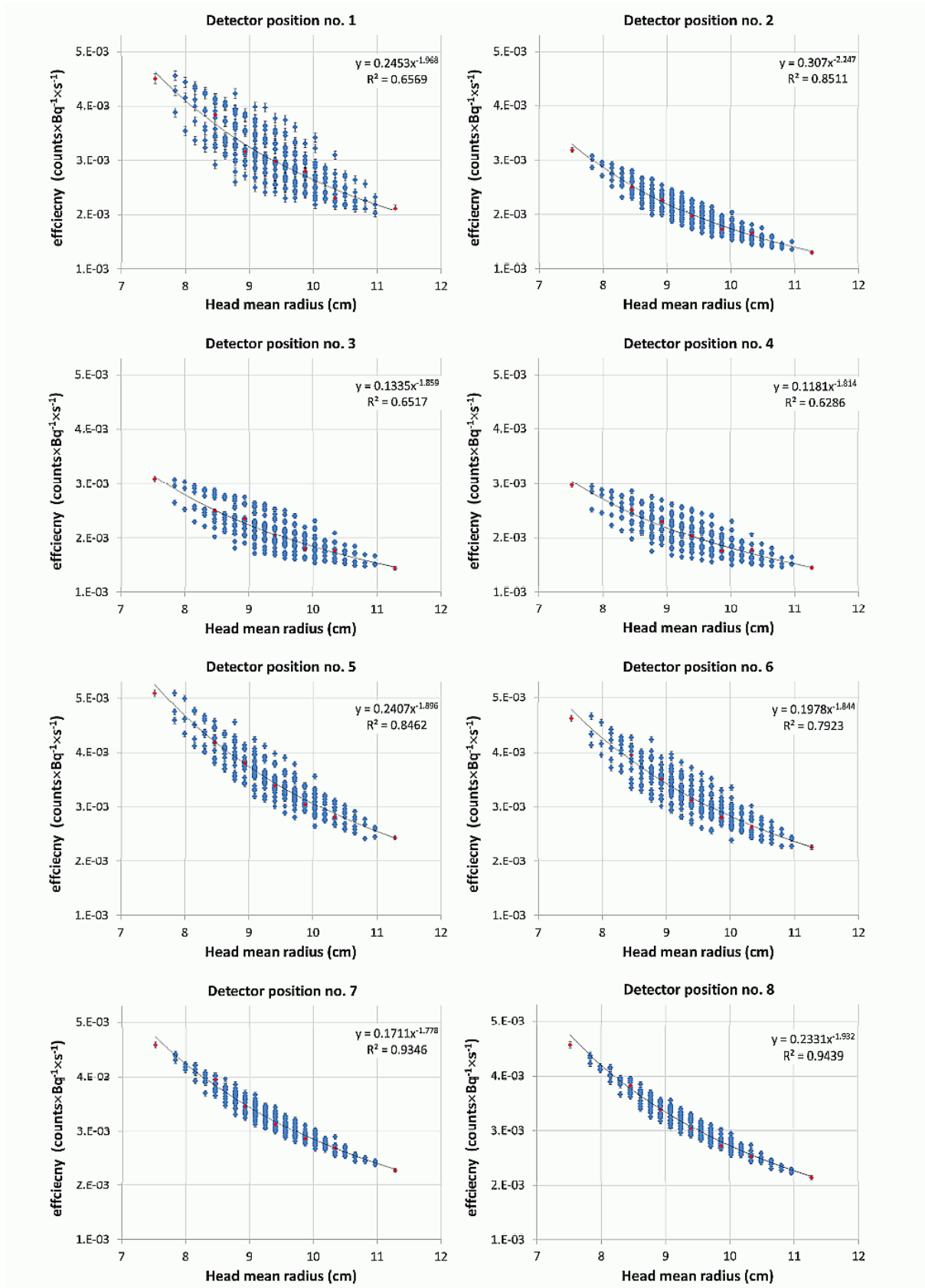


Figure 3 Detection efficiency for detector position as a function of mean head radius

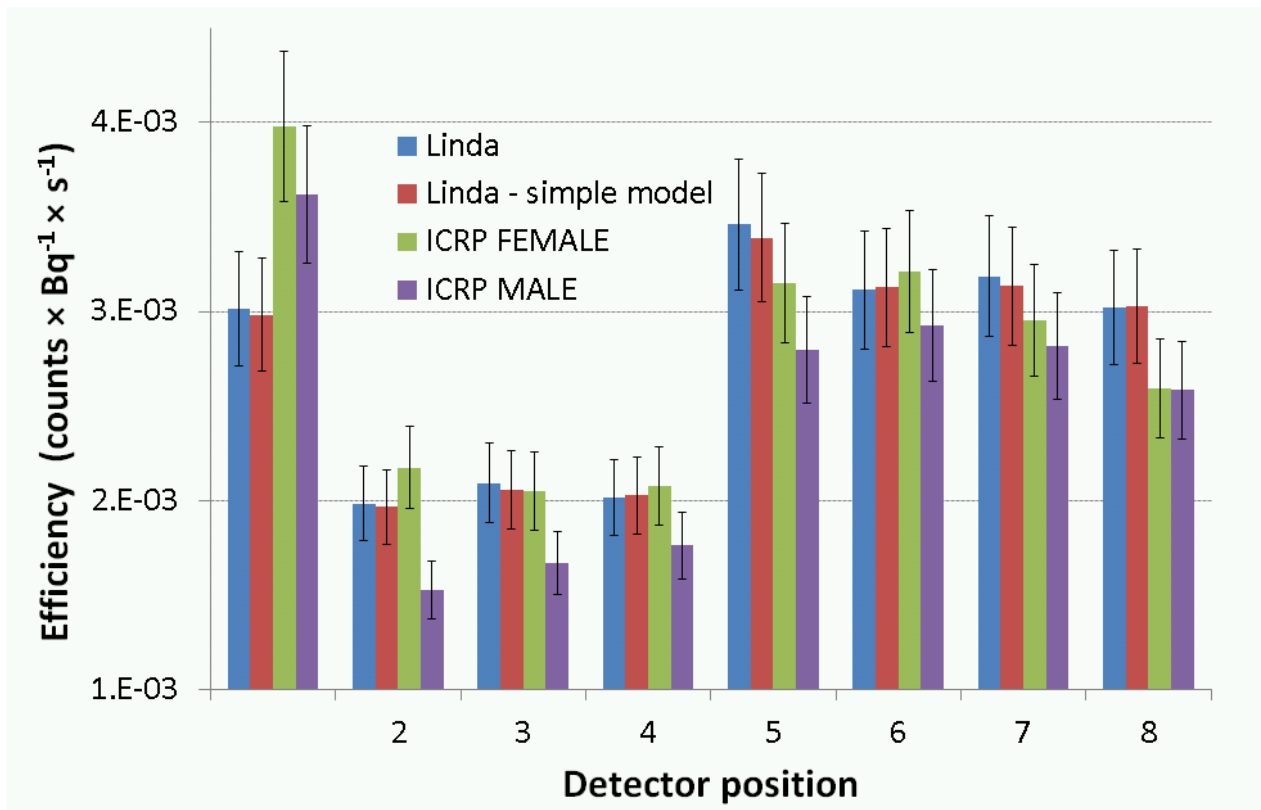


Figure 4 Phantom efficiency comparison

5 Discussion and Conclusion

The first issue needed to discuss is how the phantoms head sizes (A, B,C) are fitting mean values. The ICRP woman head is closes to the mean dimensions (A=14.49 cm, B= 19.96 cm, C=21.46 cm) (7), however its resolution is not perfect. Linda phantom is somewhat bigger than the mean head, therefore has to be altered in little bit larger interval, in order to cover possible head dimensions. Currently used interval covers from at least 5th to 95th percentile except for size A where the data starts from circa 8th percentile. More over according NASA data (8) there is significant correlation between A and B (coefficient larger than 0.6) thus it could reduce possible variation. Such arrangement will be subject of the future study.

Crucial question is accuracy of the detector setting. Limiting factor is voxel size, especially for ICRP male phantom head. Large voxel side in z axis (8 mm) makes setting quite difficult. Typical uncertainty in the detector to head distance is about ± 1 mm which is based on a personal judgment.

It could be concluded that ICRP female phantom is quite close in efficiency to previously developed Linda phantom, except for position one. Higher efficiency of the ICRP female, and also male, could be explained by insufficient covering of the top part of the head with soft tissues. The ICRP male phantom exhibits lower detection efficiency compare to both feminine model of the head. The lower detection efficiency is in agreement with decreasing trend shown in Figure 3. Difference between

Linda and ICRP male phantom falls within $\pm 10\%$ when corrected for the size, except for the 1st and 5th position. The first results on shape dependence of the detection efficiency show that the less sensitive position is frontal and dorsal one. The most significantly is affected 1st position, i.e. the detector above head. However, study with more precise model and including anthropometrical correlations is need for more accurate results.

6 Acknowledgments

This project has been supported by the research plan of the Ministry of Education, Youth and Sports of the Czech Republic No. MSM 6840770040.

7 References

1. Moraleda M, Gomez-Ros JM, Lpez MA, Navarro T, Navarro JF. A MCNP-based calibration method and a voxel phantom for in vivo monitoring of ²⁴¹Am in skull. Nuclear Instruments and Methods in Physics Research Section A: Accelerators, Spectrometers, Detectors and Associated Equipment. 2004; 526(3): p. 551-559.
2. Vrba T. Development and application of anthropomorphic voxel phantom of the head for in vivo measurement. Radiat Prot Dosimetry. 2007; 127(1-4): p. 201-204.
3. Vrba T. Uncertainty of in vivo assessment of actinides activity in human skeleton. [web] Proceedings of Third European IRPA Congress, Helsinki; 2010.
4. Petoussi-Hens N, Bolch WE, Eckerman KF, Endo A, Hertel N, Hunt J, et al. Conversion Coefficients for Radiological Protection Quantities for External Radiation Exposures. Annals of the ICRP. 2010; 40(2): p. 1-257.
5. Vrba T. Comparison of geometries for in vivo measurements of actinides in the skull. Appl Radiat Isot. 2010; 68(4-5): p. 918-921.
6. Pelowitz D. MCNPX users manual 2.6.0. 2008.
7. Algazi VR, Duda RO, Thompson DM, Avendano C. The CIPIC HRTF database. in Applications of Signal Processing to Audio and Acoustics; 2001. p. 99-102.
8. Research OA. A Handbook of anthropometric data: National Aeronautics and Space Administration, Scientific and Technical Information Office; 1978.